The characteristics of gravelly soil physical properties and their effects on permafrost dynamics: A case study on the central Qinghai-Tibetan Plateau

Shuhua Yi[1,2], Yujie He[3*], Xinlei Guo[4], Jianjun Chen[5,6], Qingbai Wu[7], Yu Qin[1], and Yongjian Ding[1,8,9]

[1.] State Key Laboratory of Cryospheric Sciences, Northwest Institute of Eco-Environment and Resources, Chinese Academy of Sciences, 320 Donggang West Road, 730000, Lanzhou, Gansu, China

[2.] School of Geographic Sciences, Nantong University, 999 Tongjing Road, Nantong, 226007, China

[3.] Chinese Research Academy of Environmental Sciences, No.8 Dayangfang, Chaoyang District, 100012, Beijing, China

[4.] Forschungszentrum Jülich GmbH, Institute of Bio- and Geosciences, Agrosphere (IBG-3), Wilhelm-Johnen-Straße, 52428 Juelich, Germany

[5.] College of Geomatics and Geoinformation, Guilin University of Technology, 12 Jiangan Road, Guilin, 541004, China

[6.] Guangxi Key Laboratory of Spatial Information and Geomatics, 12 Jiangan Road, Guilin, 541004, China

[7.] State Key Laboratory of Frozen Soil Engineering, Northwest Institute of Eco-Environment and Resources, Chinese Academy of Sciences, 320 Donggang West Road, 730000, Lanzhou, Gansu, China

[8.] Key Laboratory of Ecohydrology of Inland River Basin, Chinese Academy of Sciences, Lanzhou 730000, China

[9.] University of Chinese Academy Sciences, Beijing, 100049, China

*Co-first Author

Correspondence to: Yongjian Ding (dyj@lzb.ac.cn)

Abstract. Soils on the Qinghai-Tibetan Plateau (QTP) have distinct physical properties from agricultural soils due to weak weathering and strong erosion. These properties might affect permafrost dynamics. However, few studies have investigated both quantitatively. In this study, we selected a permafrost site on the central region of the QTP and excavated soil samples from 20 cm to 200 cm. We measured soil porosity, thermal conductivity, saturated hydraulic conductivity and matric potential in the laboratory. Finally, we ran a simulation model replacing default sand or silty clay parameters with different combinations of these measured parameters. Results showed that gravel content (diameter >2 mm) was ~55% on average in soil profile; soil porosity was less than 0.3; saturated hydraulic conductivity ranged from 0.004-0.03 mm s^{-1}; saturated matric potential ranged from -14 to -604 mm. When

1   default sand or silty clay parameters were substituted with these measured values, the model

2   errors of soil temperature, soil liquid water content, active layer depth and permafrost lower

3   boundary were reduced. The root mean squared errors of active layer depths simulated using

4   measured parameters, and the default sand and silty clay parameters were about 0.28, 1.06,

5   1.83 m, respectively. Among these measured parameters, porosities, which were much

6   smaller than soil textures used in land surface models, played a dominant role in reducing

7   model errors. We also demonstrated that soil water dynamic processes should be considered,

8   rather than using static properties under frozen and unfrozen soil states as in most permafrost

9   models. We concluded that it is necessary to consider the distinct physical properties of soil

10 and water dynamics on the QTP when simulating dynamics of permafrost in this region. It is

11 important to develop methods for systematic measuring physical properties of gravelly soil

12 and to develop a spatial dataset for porosity because of its importance in simulating

13 permafrost dynamics in this region.

14 **Key words:** Terrestrial Ecosystem Model; Active Layer; Sensitivity Test; Soil Temperature;

15 Soil Water Content; Gravel

16 **1   Introduction**

17 Permafrost covers 25% of the earth surface. Degradation of permafrost has been reported

18 extensively in Alaska, Siberia and the Qinghai-Tibetan Plateau (QTP; Boike et al., 2013;

19 Jorgenson et al., 2006; Wu and Zhang, 2010). It has global impacts by releasing large

20 quantities of soil carbon previously preserved in a frozen state and enhancing concentrations

21 of atmospheric greenhouse gases, which will promote further atmospheric warming and

22 degradation of permafrost (Anisimov, 2007; McGuire et al., 2009). Permafrost dynamics also

23 have local to regional impacts on ecosystems by altering soil thermal and hydrological

24 regimes (Salmon et al., 2015; Wang et al., 2008; Wright et al., 2009; Ye et al., 2009; Yi et al.,

25 2014a). In addition, degradation of permafrost affects infrastructure, e.g. QTP railways and

26 roads (Wu et al., 2004), and the Trans-Alaska Pipeline System in Alaska (Nelson et al., 2001).

27 Therefore, it is critical to develop mitigation and adaptation strategies in permafrost regions

28 for ongoing climate change. Accurate projection of the degree of permafrost degradation is a

29 prerequisite for developing these strategies.

30   Significant effort has been made to improve modeling accuracy and efficiency of

31 permafrost dynamics along two primary lines of inquiry. One is to create suitable freezing and

1   thawing algorithms for different applications, including land surface models (Chen et al.,

2   2015; Oleson et al., 2010; Wang et al., 2017), permafrost models (Goodrich, 1978; Langer et

3   al., 2013; Qin et al., 2017) and other related models (Fox, 1992; Woo et al., 2004). The other

4   line of inquiry is focused on schemes of soil physical properties (Chen et al., 2012; Zhang et

5   al., 2011), which play a critical role in permafrost dynamics. For example, thermal diffusivity

6   (thermal conductivity/heat capacity) directly determines how quickly energy can be

7   conducted into and out of permafrost from the top and from the bottom of the permafrost

8   horizon. Porosity determines the maximum amount of water that can be contained in a soil

9   layer, and hydraulic properties determine the exchange of soil water between soil layers. The

10 amount of water then affects not only soil thermal properties, but also determines the large

11 amount of latent heat loss/gain for freezing/thawing. On the QTP, soil is coarse due to weak

12 weathering and strong erosion (Arocena et al., 2012). Soils with gravel content (particle

13 diameter >2 mm) has been reported in several studies (Wang et al., 2011; Wu et al., 2016;

14 Yang et al., 2009; Qin et al., 2015; Chen et al., 2017; Du et al., 2017). These gravelly soil

15 properties are different from those used in current modeling studies (Wang et al., 2013). For

16 example, Soil properties in Community Land Model are calculated from fractions of sand, silt

17 and clay based on measurements of agriculture soils (Oleson et al., 2010). However, those of

18 gravelly soil on the QTP and their effects on permafrost dynamics are under studied (Pan et

19 al., 2017).

20   In this study we investigated the characteristics of soil physical properties at a site on the

21 central QTP and its effects on permafrost dynamics. We first measured soil physical properties

22 of excavated soil samples in laboratory. We then conducted sensitivity analyses with an

23 ecosystem model by substituting the default soil physical properties by those that we

24 measured. We aimed to emphasize the effects of gravel content on soil physical properties and

25 on permafrost dynamics. It is not our purpose to develop general schemes of soil physical

26 properties for using in modeling studies on the QTP.

27 **2   Methods**

28 **2.1   Site description**

29 The site (34°49'46.2" N, 92°55'56.58" E, 4,628ma.s.l.) is located in the Beiluhe basin, it is in

30 flat terrain with most slopes <10°. Fluvial and deluvial sediments formed the upland plain

31 landforms. The surficial sediments are dominated by fine to gravelly sands. (Yin, et al., 2017).

32 The site is located in the continuous permafrost region of the central QTP (Figure 1a, Zou et

al., 2017). Based on the soil map of Li et al. (2015), soil of this region belongs to Gelisols and

Inceptisols, which occupy 34% and 28% of the total area of permafrost region of the QTP,

respectively. Meteorological variables (air temperature, radiation, precipitation and humidity),

soil variables (soil temperature and moisture) down to 1.6 m, and borehole temperatures down

to 60 m have been measured at this site since 2002. The meteorological station and borehole

are located on a gentle slope with sparse vegetation (Figure 1b). Based on measurements, the

mean annual precipitation and air temperature are 366 mm yr^{-1} and -3.6 ^{o}C, respectively.

Active layer depth is ~3.3 m and the lower boundary of permafrost is at a depth of ~20 m.

Details of meteorological and borehole variables can be found in Qin et al. (2013).

2.2 Soil sampling and measurement

We excavated soil outside of the fence of the meteorological station (Figure 1b) down to 2 m

(Figure 1c) in August 2014. We used cut rings (10 cm diameter and 500 cm^{3}) to take soil

samples at depth ranges of 0-10, 10-20, 20-30, 40-50, 70-80, 110-120, 150-160, and 190-200

cm. At each depth, three replicates were sampled and sealed for analysis in the laboratory.

Above 120 cm in the soil pit, coarse soil material was small enough to be fitted in cut rings.

Below 150 cm, there exists weathered mudstone, which could also be sampled with our cut

rings.

We used the KD2 Pro (Decagon, US) to measure thermal conductivity of soil samples. The

steps were: 1) soil samples were dried in oven and weighed to calculate bulk density; 2) soil

samples were exposed to a constant temperature (20°C) over 24 h, samples were then saturated

with water (20°C) weighed (0.001g precision), and the KD2 probe (SH-1) was then inserted

into soil samples to measure thermal conductivity; 3) samples and the KD2 probe were then put

into a refrigerator (0~-26°C) at -5°C over 12 h, at which time thermal conductivity was

measured. Steps 2 and 3 were repeated at different levels of soil water content. 4) Finally, soil

samples were immersed into water over 24 h and weighed to calculate porosity; and the

saturated unfrozen and frozen thermal conductivity were then measured, accordingly.

We used pressure membrane instruments (1500F1, Soilmoisture Equipment Corp, US) to

measure matric potential of soil samples (Azam et al., 2014; Wang et al., 2007). In this study

we used both 15 bar and 5 bar pressure chamber. We used soil permeability meter (TST-70,

China) to measure saturated hydraulic conductivity of soil samples (Gwenzi et al., 2011).

1   Finally, soil samples were sieved through meshes with diameters of 2.0, 1.0, 0.5 and 0.25 mm

2   in a sequence and weighted to calculate fractions.

2.3   Model description

4   The model used in this study is dynamic organic soil version of Terrestrial Ecosystem Model

5   (DOS-TEM). Models of TEM family simulate the carbon and nitrogen pools of vegetation

6   and soil, and their fluxes among atmosphere, vegetation and soil (McGuire et al., 1992). They

7   have been widely used in studies of cold region ecosystems (e.g. McGuire et al., 2000; Yuan

8   et al., 2012; Zhuang et al., 2004; 2010) The DOS-TEM consists of four modules, these being

9   the environmental, ecological, fire disturbance, and dynamic organic soil modules (Yi et al.,

10   2010). The environmental module operates on a daily time interval using mean daily air

11   temperature, surface solar radiation, precipitation, and vapor pressure, which are downscaled

12   from monthly input data (Yi et al., 2009b). The module takes into account radiation and water

13   fluxes among the atmosphere, canopy, snow pack, and soil.

2.3.1   Implementation of soil thermal processes

15   Earlier versions of TEM did not simulate soil temperature (McGuire et al., 1992). Zhuang et

16   al. (2001) incorporated Goodrich permafrost model into TEM. Yi et al. (2009a) incorporated a

17   two-directional Stefan algorithm to simulate soil freezing and thawing for complex soil

18   situation with changes of organic soil and moisture. Soil temperatures of all soil layers in the

19   DOS-TEM are updated daily. Phase change is calculated first before heat conduction. A two-

20   directional Stefan algorithm is used to predict the depths of freezing or thawing fronts within

21   the soil (Woo et al., 2004). It first simulates the depth of the front in the soil column from the

22   top downward, using soil surface temperature as the driving temperature. It then simulates the

23   front from the bottom upward using the soil temperature at a specified depth beneath a front

24   as the driving temperature (bottom-up forcing). The latent heat used for phase change is

25   recorded for each soil layer. If a layer contains n freezing or thawing fronts, this layer is then

26   explicitly divided into $n+1$ soil layers All soil layers are grouped into 3 parts: 1) the soil layers

27   above the uppermost freezing or thawing front; 2) the soil layers below the lowermost

28   freezing or thawing front; and 3) the soil layers between the uppermost and lowermost fronts.

29   Soil temperatures are then updated by solving finite difference equations of each part with

30   phase change latent heat as energy source or sink (Yi et al., 2014a). Soil surface temperature,

1   which is used as a boundary condition, is calculated using daily air maximum, air minimum,

2   radiation, and leaf area index (Yi et al., 2013).

3   The version of the DOS-TEM in this study uses the Côté and Konard (2005) scheme to

4   calculate thermal conductivity (Yi et al., 2013; Pan et al., 2017), which is also used by other

5   studies on the QTP (e.g. Chen et al., 2012, Luo et al., 2009).

$$\lambda = \begin{cases} k_e \lambda_{sat} + (1 - k_e)\lambda_{dry} & s > 10^{-5} \\ \lambda_{dry} & s \leq 10^{-5} \end{cases} \tag{1}$$

7   where λ, λ_{sat}, λ_{dry} are soil thermal conductivity, saturated soil thermal conductivity, and dry

8   soil thermal conductivity (W m^{-1} K^{-1}), respectively.

$$\lambda_{dry} = \chi 10^{-\eta\phi} \tag{2}$$

10   where χ (W m^{-1} K^{-1}) and η (no unit) are parameters accounting for particle shape effects,

11   which are specified for gravel, fine mineral and organic soil (Côté and Konard, 2005). ϕ is

12   porosity.

$$\lambda_{sat} = \begin{cases} \lambda_s^{1-\phi} \lambda_{liq}^{\phi} & T \leq T_f \\ \lambda_s^{1-\phi} \lambda_{ice}^{\phi} & T > T_f \end{cases} \tag{3}$$

14   where λ_{liq}, λ_{ice}, λ_s are thermal conductivity of liquid water, ice and solid (W m^{-1} K^{-1}), which

15   are all constant values.

16   **2.3.2 Implementation of soil hydrological processes**

17   Surface runoff, infiltration, and water redistribution among soil layers are simulated in a

18   similar way as Community Land Model 4 (Oleson et al 2010). Soil matric potential (Ψ)

19   determines the direction of water movement. And hydraulic conductivity determines the rate

20   of water movement.

21   $\Psi = \Psi_{sat}(\frac{\theta_{liq}}{\phi})^{-B}$ (4)

22   where Ψ_{sat} is saturated soil matric potential (mm), θ_{liq} is volumetric liquid water content (m^3

23   m^{-3}), and B is pore size distribution parameter.

24   $K = K_{sat}(\frac{\theta_{liq}}{\phi})^{2B+3}$ (5)

1 where K is soil hydraulic conductivity, and K_{sat} is saturated soil hydraulic conductivity (mm s^{-1}

2).

3 Several important features relating to permafrost have been considered in the DOS-TEM

4 (see Yi et al., 2014b), e.g. runoff from perched saturated zone and exchanges of water

5 between soil and a water reservoir. Runoff from the perched saturated zone above the

6 permafrost is implemented following Swenson et al. (2013),

7 $$Q_{perch} = \alpha k_p (z_{frost} - z_{perched}) \sin(\frac{\theta}{180}\pi) \qquad (6)$$

8 Where α is an adjustable parameter (0.6 m^{-1}), K_p is the mean saturated hydraulic conductivity

9 within perched saturated zone (mm s^{-1}), z_{frost} and $z_{perched}$ are the depths to permafrost table and

10 perched water table (m), respectively, and θ is slope (^{o}).

11 The DOS-TEM has been verified against the Neumann Equation for water, mineral and

12 organic soil under an idealized condition (Yi et al., 2014b), and validated against field

13 measurements for various locations in Alaska, the Arctic, and the QTP (Yi et al., 2009b, Yi et

14 al., 2013, Yi et al., 2014a).

15 **2.4 Model inputs and initialization**

16 We used the measured air temperature, downward radiation, precipitation and humidity

17 (monthly) as input to drive the DOS-TEM. Leaf area index, one half of the total green leaf

18 area per unit ground surface area, was specified to be 0.6 m^{2}m^{-2} in July and August, 0.1 m^{2}m^{-2}

19 in April and October, and interpolated linearly in other months. It is used in the DOS-TEM to

20 calculate ground surface temperature in combination with other meteorological variables (Yi

21 et al., 2013).

22 Soil temperature and moisture were initialized at -1 ^{o}C and saturation. Sand and silty clay

23 were used in testing to represent coarse and fine soil textures, respectively, on the QTP

24 (FAO/IIASA/ISRIC/ISSCAS/JRC, 2009). The temperature gradient at the bottom of bedrock

25 was set to be 0.06 ^{o}C cm^{-1} based on borehole observations. Volumetric unfrozen liquid water

26 in winter was set to be 0.1 based on observations. The DOS-TEM was the spun up using the

27 driving data from 2003-2012 for 100 yr.

2.5 Sensitivity analyses

We considered two soil textures in the DOS-TEM, i.e. silty clay and sand. The former is considered as the major soil type of this region (Lin et al., 2011), and the latter is the coarsest soil type considered in land surface modeling (Oleson et al., 2010). We first ran the DOS-TEM using the default porosity, soil thermal conductivity (Equation 1), hydraulic conductivity (Equation 5) and matric potential schemes of these two soil types (Equation 4). The parameters Φ, Ψ_{sat}, K_{sat} and B were calculated based on soil texture used in Community Land Model (Equation 4 and 5; Oleson et al., 2010). We then substituted the original values of Φ, Ψ_{sat}, K_{sat} and B based on laboratory measurements and calibration. We did not calibrate soil thermal conductivity to retrieve parameters of Equation 2 and 3. Instead, we interpolated measured thermal conductivity over a range of the degree of saturation (0 to 1), which was used as a lookup table by the DOS-TEM. Therefore, our sensitivity analyses considered a set of 4 factors, i.e. porosity, matric potential (Ψ_{sat} and B), hydraulic conductivity (K_{sat} and B) and thermal conductivity. We also analyzed 3 different slopes (0, 5 and 10°) and 3 different soil thicknesses (3.25, 4.25 and 5.25 m) above 56 m of bed rock. There are 11 soil layers with the top 9 layers being 0.05, 0.1, 0.1, 0.2, 0.2, 0.2, 0.3, 0.3 and 0.3 m thick. The thicknesses of the bottom 2 soil layers are 0.5 and 1 m, 0.5 and 2 m, and 1.5 and 2 m for the 3.25, 4.25 and 5.25 m cases, respectively. There are 6 rock layers with thicknesses of 2, 2, 4, 8, 16 and 20 m. In summary, our sensitivity analyses with the DOS-TEM involved 288 different combinations of parameter values.

We did not measure the heat capacity of gravelly soil. The maximum and minimum heat capacities of mineral soil types considered in land surface model are 2.355 and 2.136 MJ m^{-3}, respectively. The relative difference is less than 10%. Therefore, in this study, we did not make sensitivity tests using thermal diffusivity (the ratio between thermal conductivity and heat capacity).

1 **3   Results**

2 **3.1   Soil physical properties**

3 **3.1.1   Soil porosity, particle size and bulk density**

4 The mean weight fraction of gravel (particle size diameter > 2 mm) of different soil layers

5 ranged from 0.38 to 0.65 with a mean of 0.55 (Table 1). The weight fraction of soil with

6 particle size diameter > 0.25 mm ranged from 0.77 to 0.86 with a mean of 0.84 among layers.

7 The default porosities of sand and silty clay were 37.3% and 48.1%, respectively. The mean

8 porosity of 2 m depth ranged from 21% to 30% with a mean of 27%. The mean bulk density

9 ranged from 1.61 to 1.86 g cm^{-3} with a mean of 1.74 g cm^{-3}. No significant relationships were

10 found among soil porosity, bulk density and the fraction of gravel.

11 **3.1.2   Thermal conductivity**

12 The mean unfrozen dry soil thermal conductivity of different soil layers ranged from 0.24 to

13 0.40 W m^{-2} with a mean of 0.36 W m^{-2} (Table 2). The mean frozen dry soil thermal

14 conductivity ranged from 0.25 to 0.41 W m^{-2} with a mean of 0.35 W m^{-2}. The difference of

15 dry thermal conductivity between frozen and unfrozen states was small. The mean unfrozen

16 saturated soil thermal conductivity of different soil layers ranged from 2.15 to 2.74 W m^{-2}

17 with a mean of 2.48 W m^{-2} (Table 2). The mean frozen saturated soil thermal conductivity

18 ranged from 3.06 to 3.72 W m^{-2} with a mean of 3.33 W m^{-2}. The difference of saturated

19 thermal conductivity between frozen and unfrozen states was about 0.85 W m^{-2}. There existed

20 a threshold of soil wetness, below which frozen soil thermal conductivity was slightly smaller

21 than unfrozen soil (Figure 2a).

22   The default dry frozen and unfrozen thermal conductivities using Côté and Konard (2005)

23 scheme of sand and silty clay were about 0.42 and 0.22 W m^{-2}, respectively. The saturated

24 frozen and unfrozen thermal conductivities of sand were 3.11 and 1.90 W m^{-2}, respectively.

25 Those of silty clay were about 2.35 and 1.24 W m^{-2}, respectively (Figure 2b). The default dry

26 frozen and unfrozen thermal conductivities using Farouki scheme of sand and silty clay were

27 about 0.97 and 0.33 W m^{-2}, respectively. The saturated frozen and unfrozen thermal

28 conductivities of sand were 5.21 and 3.18 W m^{-2}, respectively. Those of silty clay were about

29 2.87 and 1.52 W m^{-2}, respectively (Figure 2c).

3.1.3 Saturated hydraulic conductivity

The mean saturated hydraulic conductivity of soil layers ranged from 0.0036 to 0.0315 mm s^{-1}. The maximum saturated hydraulic conductivity was about 8.7 times larger than the minimum (Table 3). The saturated hydraulic conductivity tended to be larger with increasing proportion of gravel content in the soil samples (Figure 3a), and was about 0.03-0.06 mm s^{-1} for some samples with gravel content greater than 70%. The default saturated hydraulic conductivities of sand and silty clay were 0.024 and 0.0011 mm s^{-1}, respectively.

3.1.4 Matric potential

Saturated matric potential and B were fitted using measured matric potential values. The correlation coefficients between calculated and fitted matric potential were all greater than 0.96. The mean absolute value of saturated matric potential of soil layers ranged from 27.02 to 603.7 mm, and those of B ranged from 5.22 to 1.89 (Table 3 and Figure 3b). The default absolute value of saturated matric potential of sand and silty clay were 47.29 and 632.99 mm, respectively, and the B values 3.39 and 10.38, respectively.

3.2 Comparisons between simulations using default vs. measured parameters

3.2.1 Soil temperature

The mean root mean squared errors (RMSEs) between monthly measured soil temperatures and model runs with measured parameters using different combination of soil thicknesses (3.25, 4.25 and 5.25 m) and slopes (0, 5 and 10°) were about 1.07 ^{o}C at 20 cm (Figure 4c). The mean RMSEs for all model runs with default sand and silty clay parameters were about 0.97 and 1.37 ^{o}C, respectively. For other soil layers, the RMSEs of model runs with measured parameters were much smaller than those with default sand and silty clay parameters (Figure 4d-l). The simulated soil temperatures using default sand and silty clay parameters were all lower than measured ones in summer at 100 and 200 cm; and in winter at 400 cm. The RMSEs can be as large as 2.91 ^{o}C (Figure 4e).

The standard deviations of soil temperatures among different slopes and soil thicknesses using measured parameters were larger than those using the default parameters (Figure 4); and they increased from 0.40 ^{o}C at 100 cm to 0.61 ^{o}C at 200 cm (Figure 4f and i). The standard

1 deviations using default silty clay parameters were smaller (<0.06 °C at all depths) than those

2 using default sand parameters.

3.2.2 Soil liquid water

4 The mean RMSEs between monthly measured liquid soil volumetric water content (VWC)

5 and model simulations with measured parameters ranged from 0.03 to 0.09, which were

6 smaller than RMSEs for sand and silty clay parameters (Figure 5). The model simulations for

7 silty clay parameters have larger RMSEs than those for sand parameters. VWCs were always

8 overestimated in warm seasons at depths of 10, 40 and 80 cm. VWCs were underestimated at

9 a depth of 160 cm, where the simulated soil was frozen. All model simulations overestimated

10 VWC at 40 cm, where the maximum measured VWCs were about 0.1 (Figure 5d-f).

11 The standard deviations of VWC among different slopes and soil thicknesses using sand

12 parameters were about 0.077, which were larger than those using measured parameters

13 (~0.062). The standard deviations of VWC using silty clay parameters (<0.011) were less than

14 those using measured parameters.

3.2.3 Active layer depth (ALD)

16 The mean RMSEs between measured ALDs (derived from linear interpolation of soil

17 temperatures) and modelled ALDs (simulated explicitly) were about 1.06, 1.83 and 0.28 m for

18 model runs with sand, silty clay and measured parameters (Figure 6a). The mean standard

19 deviations were about 0.088, 0.007 and 0.28 m. All simulations using sand and silty clay

20 parameters underestimated ALDs.

3.2.4 Permafrost lower boundary (PLB)

22 The mean RMSEs between measured PLBs (derived from linear interpolation of temperatures)

23 and modelled PLBs (derived from linear interpolation of simulated bed rock temperatures)

24 were about 10.25, 7.96 and 6.71 m for model runs with sand, silty clay and measured

25 parameters (Figure 6b). The mean standard deviations were about 1.89, 0.29 and 6.62 m. All

26 simulations using sand and silty clay parameters overestimated PLBs.

3.3 Model sensitivity analyses

Deep soil layers used in models are usually specified as being thick. For example, a 1 m thick soil layer was used in our simulations starting around 3 m soil depth. Soil temperatures at this depth are usually close to 0°C. Therefore, the RMSEs of deep soil layers were small and did not facilitate evaluation of model sensitivities. In the following subsections, we used 20 and 100 cm soil temperatures, ALDs and PLBs for sensitivity analysis.

3.3.1 Effects of single parameter sensitivity analyses

Porosity

Replacing default sand or silty clay porosity with measured porosities changed mean RMSEs of soil temperatures (model runs with 3 different slopes and 3 different soil thicknesses at 2 different soil depths) from 1.18 or 2.11 °C to 1.25 or 1.08 °C, respectively (Figure 7 and 8). Mean RMSEs of ALD were reduced from 1.06 or 1.84 m to 0.22 or 0.83 m, respectively. Mean RMSEs of PLB were changed from 10.26 or 7.96 m to 6.61 or 10.26 m. Mean RMSEs of VWC were reduced from 0.074 or 0.20 to 0.06 or 0.073 when measured porosities were used for replacing default sand or silty clay porosity, respectively (Figure 9 and 10).

Thermal conductivity

Replacing default sand or silty clay thermal conductivity with measured thermal conductivity reduced mean RMSEs of soil temperatures from 1.18 or 2.11°C to 1.02 or 1.33°C, respectively (Figure 7 and 8). Mean RMSEs of ALD were reduced from 1.06 or 1.84 m to 0.56 or 1.18 m, respectively. Mean RMSEs of PLB were changed from 10.26 or 7.96 m to 4.18 or 2.54 m, respectively. Mean RMSEs of VWC changed very slightly (Figure 9 and 10).

Hydraulic conductivity/Matric potential

Replacing default sand or silty clay hydraulic conductivity with measured parameters had very small effects on mean RMSEs of soil temperatures and ALDs (Figure 7 and 8). The same was true for matric potential. When hydraulic conductivity of default sand or silty clay was substituted, mean RMSEs of PLB were decreased or increased, however, when matric potential was substituted, mean RMSEs of PLBs were increased or decreased, respectively. When hydraulic conductivity or matric potential parameters were substituted in default sand or silty clay parameters, mean RMSEs of VWC changed slightly (Figure 9 and 10).

3.3.2 Effects of combined parameters

We compared model simulations with different combinations of measured parameters (porosity, thermal conductivity, hydraulic conductivity and matric potential) with those with one substituted measured parameter. We selected those model runs with less RMSEs than any of model runs with one substituted measured parameter (Table 4 and 5). We didn't consider the 10 cm soil temperature, which were similar among all model runs.

For sand, model simulations with porosity and thermal conductivity or hydraulic conductivity substituted had 4 outcomes with lower RMSEs (Table 4 and Figures 7 and 9). Only 2 out of 7 outcomes had lower RMSEs with all 4 parameters were substituted. Among all the 18 cases with RMSEs less than the individual "best" RMSE, porosity was included 18 times, followed by thermal conductivity and hydraulic conductivity with 10 times.

For silty clay, model simulations with porosity and thermal conductivity and/or matric potential substituted had 5 outcomes with lower RMSEs (Table 5 and Figures 8 and 10). Among all the 29 cases with RMSEs less than the individual "best" RMSE, porosity was included 29 times, followed by thermal conductivity with 20 times and matric potential with 16 times.

3.3.3 Effects of slope and soil thickness

Changes of slope alone had small effects on simulated soil temperatures and ALDs (Figures 7 and 8). An increase of slope generally reduced RMSEs of VWCs (Figures 9 and 10). Model simulations with porosity substituted had smaller difference of VWC RMSE between different cases of slopes. For example, the mean RMSEs of model simulations with slope of 0° or 5° and porosity substituted in default sand parameters were 0.078 or 0.048, respectively. While those with porosity not substituted were 0.141 or 0.055, respectively. Similarly, the mean RMSEs of model simulations using default silty clay parameters with porosity substituted were 0.081 or 0.06 for slope of 0° or 5°, respectively. The mean RMSEs were 0.21 or 0.138 with porosity not substituted, respectively. For a further increase of slope to 10°, changes of RMSEs of VWCs at depths of 10-160 cm were small.

Soil thickness had small effects on 20 and 100 cm soil temperatures and 10-160 cm VWCs, and it had prominent effects on PLB for a few cases only with a slope of 10° (Figures 7 and 8).

1 **4   Discussion**

2 **4.1   Characteristics of soil physical properties**

3 Although the effects of gravelly soil on permafrost dynamics have been considered in a few

4 modelling studies, the thermal and hydraulic properties of gravelly soil were calculated

5 without validation or calibrated (Pan et al., 2017; Wu et al., 2018). To our knowledge, this is

6 the first study measuring physical properties of gravelly soil samples from permafrost region

7 of the QTP.

8   The weight fraction of gravel (diameter > 2mm) in the soil samples we analysed was

9 greater than 55% on average. While the typical soil types considered in land surface models

10 and other models usually have much smaller diameter. For comparison, the fractions of gravel

11 considered in Pan et al. (2017) ranges from 5% to 33% and from 10% to 28% for the Madoi

12 and Naqu sites, respectively. The Beiluhe site and the aforementioned sites are located in

13 regions with Gelisols and Inceptisols, which occupy ~62% of the permafrost regions of the

14 QTP (Li et al., 2015). It is possible that gravelly soil commonly exists on the QTP. The

15 saturated hydraulic conductivity and matric potential of soil samples measured in this study

16 were more similar to sand than to silty clay (see Section 3.1). It is consistent with the study of

17 Wang et al. (2013) that coarse soil material has poor water holding capability.

18   The measured saturated thermal conductivities of soil samples were relatively close to

19 those estimated by the Côté and Konard (2005) scheme. But they were much less than those

20 estimated by the Farouki scheme (Figure 2). Several other studies also found that Farouki

21 scheme overestimated soil thermal conductivity (Chen et al. 2012; Luo et al., 2009).

22   One important finding of this study is the relatively small value of porosity. The measured

23 porosity ranged from 0.206 to 0.302, which is less than those of soil types considered in land

24 surface models. For example, the porosities of mineral soil types considered in Community

25 Land Model range from 0.37 to 0.48 (Oleson et al., 2010). Porosity determines the maximum

26 water stored in a soil layer, and affects soil thermal conductivity, hydraulic conductivity and

27 matric potential (Equation 2-5). It plays a more important role than other parameters in

28 simulated soil thermal and hydrological dynamics (Table 4 and 5; Figure 7-10). It is

29 noteworthy that it is easy and efficient to measure porosity.

4.2 Effects of soil water on permafrost dynamics

Soil water not only affects soil thermal properties, e.g. thermal conductivity and heat capacity, but also affects the amount of latent heat lost or gained, for freezing or thawing, respectively (Goodrich, 1978; Farouki, 1986). Soil water is determined by infiltration, evapotranspiration, water movement among soil layers, subsurface runoff and exchange with a water reservoir. Therefore, processes or parameters that affect soil water dynamics will also affect permafrost dynamics. This study quantitatively assessed the effects of soil water on permafrost dynamics. For example, when default silty clay parameters with high porosity and low saturated hydraulic conductivity were used, soil layers were almost saturated (Figure 5). The simulated ALDs were about 1.47 m, which was less than half of measured ALDs (Figure 6a). When the slope was 0°, subsurface runoff didn't happen in saturated zone above the bottom of the active layer. The simulated soil water content was generally higher in the active layer. However, when the slope was 5°, the simulated soil water content was less and the RMSE was smaller (Figure 9 and 10). These patterns were especially obvious when both porosity and saturated hydraulic conductivity were large (Equation 6; Figure 9 and 10). Other studies have also emphasized the importance of subsurface runoff above the bottom of the active layer (Frey and McClelland, 2009; Walvoord and Striegl, 2007). The effects of soil water content on soil thermal dynamics increased with soil and rock depth (Figure 7 and 8). The biggest effects were on PLB, which became manifest during long-term spinup procedures.

Land surface models generally represent soil water dynamics (e.g. Chen et al., 2015; Oleson et al., 2010; Wang et al., 2017). However the permafrost processes in these models usually use specified thermal properties, which were static during model simulations (Li et al., 2009; Nan et al., 2005; Qin et al., 2017; Zou et al., 2017). As shown in this study, when permafrost degraded, the thermal and hydrological regimes of soil also changed. It is critical to simulate soil water dynamics to properly project permafrost dynamics in the future.

4.3 Limitations and Outlook

4.3.1 Sampling and laboratory measurement

We used cut rings with 10 cm diameter to take soil samples. There are weathered mudstones in our study site, which can be sampled in cut rings. However, it is very likely that there are

1   soil samples with much bigger gravels. Therefore, larger containers should be used to take

2   samples for further laboratory analysis in the future.

3   During our laboratory work, we found two phenomena. First, we originally used the QL-

4   30 thermophysical instrument to measure thermal conductivity. It worked properly under

5   unfrozen condition. However, when frozen, surface of soil samples was uneven due to frost

6   heave. The contact between plate of QL-30 and soil sample surface was not ideal. The

7   measured frozen thermal conductivities were smaller than unfrozen thermal conductivity even

8   for the case of saturation, which were definitely wrong. The second phenomenon was that

9   there seems to be a threshold of soil wetness, below which unfrozen soil thermal conductivity

10   is greater than frozen soil thermal conductivity (Figure 2a). This pattern was somewhat

11   exhibited in estimates of the Côté and Konard (2005) scheme, but not in the estimates of the

12   Farouki scheme (Figure 2c). More measurements using instruments with higher accuracy

13   should be made in the future.

14   4.3.2   Model simulation

15   Although the DOS-TEM using measured parameters provided satisfactory results, there are

16   some aspects requiring further improvement in the future. For example, the measured soil

17   moistures at 40 cm depth were less than 0.1 m^3/m^3. However, the simulated soil moistures

18   were always much greater (Figure 5f). There were spikes of measured soil moistures at 80 and

19   160 cm depths, which were not presented in simulation (Figure 5 i and l). In the DOS-TEM,

20   the unfrozen soil water content, or supercold water, was prescribed to be 0.1 m^3/m^3. When

21   soil is freezing, if soil liquid water content is less than this value, no phase change will happen

22   (Figure 5k). It is ideal to simulate the dynamics of unfrozen soil water content (Romanovsky

23   and Osterkamp, 2000).

24   Field studies have shown that gravel content in root zone affects vegetation growth (Qin et al.,

25   2015), which affects ground surface temperature (Yi et al., 2013). In the current study, we

26   used specified leaf area index. The fractions of gravel content in soil are also dynamic. For

27   example, Chen et al. (2017) found that plateau pika excavated subsurface soil with gravel on

28   to surface. Fine soil particles were carried away by wind and water erosion, which resulted in

29   gravel remaining at the surface. Our ongoing research is working towards representing the

30   coupling of vegetation growth, small mammal disturbances, and soil erosion on permafrost

31   dynamics of the QTP in the future.

4.3.3 Regional applications

Soil texture playes an important role in permafrost dynamics (Figure 6). However, the dominant soil texture on the QTP from FAO/IIASA/ISRIC/ISSCAS/JRC (2009) is silty clay. The specification of silty clay in simulations results in estimates of ALD that are much smaller than meansurements (Yi et al., 2014a). To properly simulate the distribution and dynamics of permafrost on the QTP under climate change scenarios, it is important to develop proper schemes of soil physical properties in relation to gravel content and to develop regional datasets of soil texture for input.

Gravel content affects soil physical properties. For example, soil porosity and saturated hydraulic conductivity are determined by the fraction of gravel, diameter and degree of mixture (Zhang et al., 2011). Organic soil carbon content in mineral soil on the QTP affects soil porosity and thermal conductivity (Chen et al., 2012). We only measured physical properties of soil samples from one site on the QTP in this study. The mean gravel fraction was about 0.55, which is definitely not suitable for direct use in regional simulations. More laboratory work is needed to develop proper schemes for representing mixed soil with fine mineral, gravel and organic carbon in permafrost models. It is the first priority to develop schemes that make use of porosity data sets, due to its importance and simplicity of measurement.

The development of a spatially explicit dataset of soil texture is also required for regional applications of projecting permafrost changes on the QTP. One way is to collect relevant data through extensive field campaigns (e.g., Li et al., 2015). Currently, gravelly soil has only been mentioned in scientific literature on the QTP (Chen et al., 2015; Wang et al., 2011; Yang et al., 2009), and no systematic analysis of gravelly soils exists across the QTP. Ground penetrating radar is a feasible tool to retrieve soil thickness above gravel layer (Han et al., 2016). Unmanned aerial vehicles has been used recently (Yi, 2017), and gravel on the ground surface can be identified easily in aerial photos (Chen et al., 2017). In combination with ancillary datasets, e.g. geomorphology, topography, vegetation, it is possible to generate spatial datasets of soil texture (Li et al., 2015; Wu et al., 2016). Another way is to retrieve soil physical properties using data assimilation technology, e.g. Yang et al. (2016) assimilated porosity using a land surface model and microwave data.

1 **5 Conclusions**

2 In this study, we excavated soil samples from a permafrost site on the central QTP and

3 measured soil physical properties in laboratory. Gravel was common in the soil profile and

4 porosity was much smaller than the typical soil types used in land surface models. We then

5 performed sensitivity analysis of these parameters on soil thermal and hydrological processes

6 within a terrestrial ecosystem model. When default sand or silty clay parameters were

7 substituted with measured soil properties, the model errors of soil temperature, soil liquid

8 water content, active layer depth and permafrost low boundary were generally reduced.

9 Sensitivity analyses showed that porosity played a more important role in reducing model

10 errors than other soil properties examined. Though it is unclear how representative this soil is

11 in the QTP, it is clear that soil physical properties specific to the QTP should be used to

12 properly project permafrost dynamics into the future.

13 *Acknowledgements.* We would like to thank Prof. Dave McGuire of University of Alaska

14 Fairbanks for his careful editing. This study was jointly supported through grants provided as

15 part of the National Natural Science Foundation Commission (41422102, 41730751 and

16 41690142).

17 **References**

18 Anisimov, O. A.: Potential feedback of thawing permafrost to the global climate system

19   through methan emission, Environ. Res. Lett., 2, 1-7, 2007.

20 Arocena, J., K. Hall, and L.P.: Zhu Soil formation in high elevation and permafrost areas in

21   the Qinghai Plateau (China), Spanish Journal of Soil Sciences, 2, 34-49, 2012.

22 Azam, G., Grant, C. D., Murray, R. S., Nuberg, I. K.,and Misra, R. K. : Comparison of the

23   penetration of primary and lateral roots of pea and different tree seedlings growing in

24   hard soils. Soil Research, 52, 87-96, 2014.

25 Boike, J., Kattenstroth, B., Abramova, E., Bornemann, N., Chetverova, A., Fedorova, I., and

26   Langer, M.: Baseline characteristics of climate, permafrost and land cover from a new

27   permafrost observatory in the Lena River Delta, Siberia (1998-2011),Biogeosciences

28   (BG), 10,2105-2128, 2013.

1 Chen, H., Nan, Z., Zhao, L., Ding, Y., Chen, J., & Pang, Q.: Noah Modelling of the
2   Permafrost Distribution and Characteristics in the West Kunlun Area, Qinghai-Tibet
3   Plateau, China. Permafrost Periglac, 26,160-174, 2015.

4 Chen, J., Yi, S., and Qin, Y.: The contribution of plateau pika disturbance and erosion on
5   patchy alpine grassland soil on the Qinghai-Tibetan Plateau: Implications for grassland
6   restoration. Geoderma, 297, 1-9, 2017.

7 Chen, Y., Yang, K., Tang, W., Qin, J., and Zhao, L.: Parameterizing soil organic carbon's
8   impacts on soil porosity and thermal parameters for Eastern Tibet grasslands, Science in
9   China Series D: Earth Sciences (EN), 55, 1001-1011, 2012.

11 Cote, J. and J. Konrad: A generalized thermal conductivity model for soils and construction
12   materials, Can. Geotech. J., 42, 443-458, 2005.

13 Du, Z., Y. Cai, Y. Yan, and X. Wang: Embedded rock fragments affect alpine steppe plant
14   growth, soil carbon and nitrogen in the northern Tibetan Plateau, Plant Soil, 420, 79-92,
15   2017.

16 FAO/IIASA/ISRIC/ISSCAS/JRC: Harmonized World Soil Database (version 1.1).F669 AO,
17   Rome, Italy and IIASA, Laxenburg, Austria, 2009.

18 Farouki, O. T.:Thermal properties of soils, Cold Reg. Res. and Eng. Lab., Hanover, N. H,
19   1986.

20 Fox, J. D.: Incorporating Freeze-Thaw Calculations into a water balance model, Water Resour.
21   Res., 28, 2229-2244, 1992.

22 Frey, K. E., and McClelland, J. W.: Impacts of permafrost degradation on arctic river
23   biogeochemistry, Hydrol. Process, 23, 169-182, 2009.

24 Goodrich, E. L.: Efficient Numerical Technique for one-dimensional Thermal Problems with
25   phase change, Int. J. Heat Mass Transfer, 21, 615-621, 1978.

26 Gwenzi, W., Hinz, C., Holmes, K., Phillips, I. R., and Mullins, I. J.: Field-scale spatial
27   variability of saturated hydraulic conductivity on a recently constructed artificial
28   ecosystem, Geoderma, 166, 43-56, 2011.

29 Han.X., Liu, J. , Zhang, J., and Zhang, Z.: Identifying soil structure along headwater
30   hillslopes using ground penetrating radar based technique. Journal of Mountain
31   Science, 13, 405-415, 2016.

32 Jorgenson, M. T., Shur, Y. L., and Pullman, E. R.: Abrupt increase in permafrost degradation
33   in Arctic Alaska, Res. Lett., 33, L02503, doi:10.1029/2005GL024960, 2006.

1   Langer, M., Westermann, S., Heikenfeld, M., Dorn, W., and Boike, J.: Satellite-based
2   modeling of permafrost temperatures in a tundra lowland landscape, Remote Sensing of
3   Environment, 135, 12-24, 2013.
4   Li, J., Sheng, Y., Wu, J., Chen, J., and Zhang, X.: Probability distribution of permafrost along
5   a transportation corridor in the northeastern Qinghai province of China. Cold Regions
6   Science and Technology, 59, 12-18, 2009.
7   Li, W., L. Zhao, X. Wu, Y. Zhao, H. Fang, and W. Shi: Distribution of soils and landform
8   relationships in the permafrost regions of Qinghai-Xizang (Tibetan) Plateau, Chinese Sci.
9   Bull., 23, 2216-2226, 2015.
10 Lin, Z., F. Niu, H. Liu, and J. Lu: Hydrothermal processes of alpine tundra lakes, Beiluhe
11   Basin, Qinghai-Tibet Plateau, Cold Reg. Sci. Techol., 65, 446-455, 2011.
12 Luo, S., Lv, S., Zhang, Y., Hu, Z., Ma, Y., Li, S., and Shang, L.: Soil thermal conductivity
13   parameterization establishment and application in numerical model of central Tibetan
14   Plateau, Chinese Journal of Geophysics, 52, 919-928, 2009. (in Chinese with English
15   Abstract)
16 McGuire, A. D., J. Melillo, E. G. Jobbagy, D. Kicklighter, A. L. Grace, B. Moore, and C. J.
17   Vorosmarty: Interactions Between Carbon and Nitrogen Dynamics in Estimating Net
18   Primary Productivity for Potential Vegetation in North America, Global Biogeochem. Cy.,
19   6(2), 101-124, 1992.
20 McGuire, A. D., J. S. Clein, J. Melillo, D. Kicklighter, R. A. Meier, C. J. Vorosmarty, and M.
21   C. Serreze: Modelling carbon responses of tundra ecosystems to historical and projected
22   climate: sensitivity of pan-Arctic carbon storage to temporal and spatial variation in
23   climate, Global Change Biol., 6 (Suppl. 1), 141-159, 2000.
24 McGuire, A. D., Anderson, L. G., Christensen, T. R., Dallimore, S., Guo, L., Hayes, D. J., .
25   and Roulet, N.: Sensitivity of the carbon cycle in the Arctic to climate change. Ecological
26   Monographs, 79, 523-555, 2009.
27 Nan, Z., Li, S., and Cheng, G.: Prediction of permafrost distribution on the Qinghai-Tibet
28   Plateau in the next 50 and 100 years. Science in China Series D: Earth Sciences, 48, 797-
29   804, 2005.
30 Nelson, F. E., Anisimov, O. A.,and Shiklomanov, N. I.: Subsidence risk from thawing
31   permafrost, Nature, 410(6831), 889-890, 2001.
32 Oleson, K. W., Lawrence, D. M., Bonan, G. B., Flanner, M. G., Kluzek, E., Lawrence, P. J.,
33   Levis, S., Swenson, S. C., and Thornton, P.: Technical description of version 4.0 of the

1   Community Land Model (CLM), University Corporation for Atmospheric Research,
2   NCAR 2153-2400, 2010.

3   Pan, Y., S. Lv, S. Li, Y. Gao, X. Meng, Y. Ao, and S. Wang: Simulating the role of gravel in
4   freeze–thaw processon the Qinghai–Tibet Plateau, Theor. Appl. Climatol., 127, 1011-
5   1022, 2017.

6   Qin, Y., J. E. Hiller, G. Jiang, and T. Bao: Sensitivity of thermal parameters affecting cold-
7   region ground-temperature predictions, Environ. Earth Sci., 68, 1757-1772, 2013.

8   Qin Y., Wu, T. , Zhao, L., Wu, X., Li, R., Xie, C., Pang, Q., Hu, G., Qiao, Y., Zhao, G., Liu,
9   G., Zhu, X., and Hao, J.: Numerical Modeling of the Active Layer Thickness and
10   Permafrost Thermal State Across Qinghai-Tibetan Plateau, Journal of Geophysical
11   Research: Atmospheres, doi:10.1002/2017JD026858, 2017.

12   Qin, Y., Yi, S., Chen, J., Ren, S., and Ding, Y.: Effects of gravel on soil and vegetation
13   properties of alpine grassland on the Qinghai-Tibetan plateau. Ecological Engineering, 74,
14   351-355, 2015.

15   Romanovsky, V. E. and T. E. Osterkamp: Effects of unfrozen water on heat and mass
16   transport processes in the active layer and permafrost, Permafrost Periglac., 11, 219-239,
17   2000.

18   Salmon, V. G., Soucy, P., Mauritz, M., Celis, G., Natali, S. M., Mack, M. C., & Schuur, E. A.:
19   Nitrogen availability increases in a tundra ecosystem during five years of experimental
20   permafrost thaw, Global Change Biol., 22, 1927-1941, 2016.

21   Swenson, S. C., D. M. Lawrence, and H. Lee: Improved simulation of the terrestrial
22   hydrological cycle in permafrost regions by the Community Land Model, Journal of
23   Advances in Modeling Earth Systems, 4, M08002, doi:10.1029/2012MS000165, 2013.

24   Walvoord, M. A., & Striegl, R. G.: Increased groundwater to stream discharge from
25   permafrost thawing in the Yukon River basin: Potential impacts on lateral export of
26   carbon and nitrogen. Geophys. Res. Lett., 34, L12402, doi:10.1029/2007GL030216, 2007.

27   Wang, F. X., Kang, Y., Liu, S. P., & Hou, X. Y.: Effects of soil matric potential on potato
28   growth under drip irrigation in the North China Plain. Agricultural water management, 88,
29   34-42, 2007.

30   Wang, H., B. Xiao, M. Wang, and Ming'an Shao: Modeling the soil water retention curves of
31   soil-gravel mixtures with regression method on the Loess Plateau of China, PLoS ONE, 8,
32   e59475, doi:10.1371/journal.pone.0059475, 2013.

1 Wang, G., Li. Y., Wang. Y., and Wu, Q.: Effects of permafrost thawing on vegetation and soil
2   carbon pool losses on the Qinghai-Tibet Plateau, China, Geoderma, 143, 143-152,2008.
3 Wang, L., Zhou, J., Qi, J., Sun, L., Yang, K., Tian, L., and Koike, T.: Development of a land
4   surface model with coupled snow and frozen soil physics, Water Resources Research, 53,
5   5085-5103, doi:10.1002/2017WR020451, 2017.
6 Wang, X., Liu, G., and Liu, S.: Effects of gravel on grassland soil carbon and nitrogen in the
7   arid regions of the Tibetan Plateau. Geoderma, 166, 181-188, 2011.
8 Woo, M. K., Arain, M. A., Mollinga, M., and Yi, S.: A two-directional freeze and thaw
9   algorithm for hydrologic and land surface modelling. Geophys. Res. Lett., 31, L12501,
10   doi:10.1029/2004GL019475, 2004.
11 Wright, N., Hayashi, M., & Quinton, W. L.: Spatial and temporal variations in active layer
12   thawing and their implication on runoff generation in peat-covered permafrost
13   terrain. Water Resour. Res., 45, W05414, doi:10.1029/2008WR006880, 2009.
14 Wu, Q., Cheng, G., and Ma, W.: Impact of permafrost change on the Qinghai-Tibet Railroad
15   engineering. Science in China Series D: Earth Sciences, 47, 122-130, 2004.
16 Wu, Q., and Zhang, T.:. Changes in active layer thickness over the Qinghai-Tibetan Plateau
17   from 1995 to 2007. J. Geophys. Res., 115, D09107, doi:10.1029/2009JD012974, 2010.
18 Wu, X., Zhao, L., Fang, H., Zhao, Y., Smoak, J. M., Pang, Q., and Ding, Y.: Environmental
19   controls on soil organic carbon and nitrogen stocks in the high-altitude arid western
20   Qinghai-Tibetan Plateau permafrost region, J. Geophys. Res., 121, 176-187, 2016.
21 Wu, X., Z. Nan, S. Zhao, L. Zhao, and G. Cheng: Spatial modeling of permafrost distribution
22   and properties on the Qinghai-Tibetan Plateau, Permafrost Periglac., DOI:
23   10.1002/ppp.1971, 2018
24 Yang, J., Mi, R., & Liu, J.:Variations in soil properties and their effect on subsurface biomass
25   distribution in four alpine meadows of the hinterland of the Tibetan Plateau of China,
26   Environ. Geol., 57, 1881-1891, 2009.
27 Yang, K., Zhu, L., Chen, Y., Zhao, L., Qin, J., Lu, H., ... and Fang, N.: Land surface model
28   calibration through microwave data assimilation for improving soil moisture
29   simulations,Journal of Hydrology, 533, 266-276, 2016.
30 Ye, B., Yang, D., Zhang, Z., and Kane, D. L.: Variation of hydrological regime with
31   permafrost coverage over Lena Basin in Siberia. J. Geophys. Res., 114, D07102,
32   doi:10.1029/2008JD010537, 2009.

1   Yi S, FragMAP: a tool for long-term and cooperative monitoring and analysis of small-scale
2   habitat fragmentation using an unmanned aerial vehicle, International Journal of Remote
3   Sensing, 38:2686-2697, 2017.

4   Yi, S., Manies, K. L., Harden, J., and McGuire, A. D.: The characteristics of organic soil in
5   black spruce forests: Implications for the application of land surface and ecosystem
6   models in cold regions, Geophys. Res. Lett., 36, L05501, doi:10.1029/2008GL037014,
7   2009a.

8   Yi, S., McGuire, A. D., Harden, J., Kasischke, E., Manies, K. L., Hinzman, L. D., Liljedahl,
9   A., Randerson, J. T., Liu, H., Romanovsky, V. E., Marchenko, S., and Kim, Y.:
10   Interactions between soil thermal and hydrological dynamics in the response of Alaska
11   ecosystems to fire disturbance , J. Geophys. Res., 114, G02015,
12   doi:10.1029/2008JG000841, 2009b.

13   Yi, S., McGuire, A. D., Kasischke, E., Harden, J., Manies, K. L., Mack, M., and Turetsky, M.
14   R.: A Dynamic organic soil biogeochemical model for simulating the effects of wildfire
15   on soil environmental conditions and carbon dynamics of black spruce forests, J.
16   Geophys. Res., 115, G04015, doi:10.1029/2010JG001302, 2010.

17   Yi. S., Li, N., Xiang, B., Ye, B. and McGuire, A.D.: Representing the effects of alpine
18   grassland vegetation cover on the simulation of soil thermal dynamics by ecosystem
19   models applied to the Qinghai-Tibetan Plateau, J. Geophys. Res., 118, 1-14, doi:
20   10.1002/jgrg.20093, 2013.Yi, S., Wang, X., Qin, Y., Xiang, B., and Ding, Y.: Responses
21   of alpine grassland on Qinghai–Tibetan plateau to climate warming and permafrost
22   degradation: a modeling perspective. Environ. Res. Lett., 9, 074014, doi:10.1088/1748-
23   9326/9/7/074014, 2014a.

24   Yi, S., Wischnewski, K., Langer, M., Muster, S., Boike, J.: Modeling different freeze/thaw
25   processes in heterogeneous landscapes of the Arctic polygonal tundra using an ecosystem
26   model. Geoscientific Model Development, 7, 1671–1689, 2014b.

27   Yin, G., Niu, F., Lin, Z., Luo, J., and Liu, M.: Effects of local factors and climate on
28   permafrost conditions and distribution in Beiluhe basin, Qinghai-Tibet Plateau, China.
29   Science of the Total Environment, 581-582, 472-485, 2017.

30   Yuan, F. M., Yi, S. H., McGuire, A. D., Johnson, K. D., Liang, J., Harden, J. W., ... and Kurz,
31   W. A.:Assessment of boreal forest historical C dynamics in the Yukon River Basin:
32   relative roles of warming and fire regime change Ecol,Appl., 22, 2091-2109, 2012.

1   Zhang, Z. F., & Ward, A. L.: Determining the porosity and saturated hydraulic conductivity
2   of binary mixtures, Vadose Zone J., 10, 313-321, 2011.
3   Zhuang, Q., V. E. Romanovsky, and A. D. McGuire: Incorporation of a permafrost model into
4   a large-scale ecosystem model: Evaluation of temporal and spatial scaling issues in
5   simulating soil thermal dynamics, J. Geophys. Res., 106(D24), 33649-33670, 2001.
6   Zhuang, Q., J. Melillo, D. Kicklighter, R. G. Prinn, A. D. McGuire, P. A. Steudler, B. S.
7   Felzer, and S. Hu: Methane fluxes between terrestrial ecosystems and the atmosphere at
8   northern high latitudes during the past century: A retrospective analysis with a process-
9   based   biogeochemistry   model,   Global   Biogeochem.   Cy.,   18,   GB3010,
10   doi:10.1029/2004GB002239, 2004.Zhuang, Q., J. He, Y. Lu, L. Ji, J. Xiao, and T. Luo:
11   Carbon dynamics of terrestrial ecosystems on the Tibetan Plateau during the 20th century:
12   an analysis with a process-based biogeochemical model, Global Ecol. Biogeogr., 19, 649-
13   662, 2010.
14 Zou, D., L. Zhao, Y. Sheng, J. Chen, G. Hu, T. Wu, J. Wu, C. Xie, X. Wu, Q. Pang, W. Wang,
15   E. Du, W. Li, G. Liu, J. Li, Y. Qin, Y. Qiao, Z. Wang, J. Shi, and G. Cheng: A new map
16   of permafrost distribution on the Tibetan Plateau, The Cryosphere, 11, 2527-2542, 2017.

1 **Table 1.** The mean (standard deviation) of measured soil bulk density, porosity, and particle
2 size diameter fractions of different layers based on soil samples in this study.

Layer (cm)	Bulk density (g cm⁻³)	Porosity (%)	Fractions of particle in each diameter range				
			>2 mm	1-2 mm	0.5-1 mm	0.25-0.5 mm	<0.25 mm
0—10	1.74 (0.21)	28.4 (0.03)	0.38 (0.07)	0.05 (0.01)	0.17 (0.10)	0.17 (0.06)	0.22 (0.08)
10—20	1.81 (0.11)	27.7 (0.02)	0.52 (0.14)	0.09 (0.04)	0.14 (0.06)	0.09 (0.02)	0.15 (0.08)
20—30	1.86 (0.32)	30.2 (0.05)	0.55 (0.17)	0.09 (0.05)	0.14 (0.12)	0.08 (0.01)	0.14 (0.02)
40—50	1.61 (0.23)	29.6 (0.02)	0.55 (0.19)	0.07 (0.04)	0.16 (0.17)	0.07 (0.04)	0.15 (0.04
70—80	1.62 (0.20)	20.6 (0.11)	0.65 (0.16)	0.06 (0.06)	0.09 (0.10)	0.08 (0.02)	0.11 (0.01)
110—120	1.75 (0.09)	27.7 (0.01)	0.63 (0.05)	0.04 (0.01)	0.06 (0.01)	0.09 (0.05)	0.18 (0.07)
150—160	1.70 (0.15)	26.3 (0.02)	0.63 (0.09)	0.04 (0.04)	0.07 (0.06)	0.10 (0.04)	0.16 (0.08)
190—200	1.81 (0.09)	27.1 (0.02)	0.50 (0.19)	0.10 (0.10)	0.14 (0.13)	0.10 (0.02)	0.16 (0.05)

1   **Table 2.** The mean (standard deviation) of the measured frozen and unfrozen dry and

2   saturated soil thermal conductivity (W m^{-2}) of different soil layers.

	Dry		Saturated	
Layer (cm)	Unfrozen	Frozen	Unfrozen	Frozen
0-10	0.238 (0.09)	0.414 (0.09)	2.322 (0.17)	3.122 (0.48)
10~20	0.340 (0.04)	0.365 (0.23)	2.147 (0.47)	3.193 (0.55)
20-30	0.395 (0.07)	0.420 (0.11)	2.743 (0.38)	3.059 (0.29)
40-50	0.346 (0.00)	0.388 (0.14)	2.539 (0.30)	3.184 (0.33)
70-80	0.340 (0.03)	0.289 (0.12)	2.589 (0.16)	3.362 (0.38)
110-120	0.400 (0.06)	0.271 (0.07)	2.616 (0.11)	3.721 (0.05)
150-160	0.401 (0.01)	0.248 (0.07)	2.246 (0.19)	3.647 (0.48)
190-200	0.399 (0.26)	0.392 (0.14)	2.609 (0.12)	3.329 (0.19)

1   **Table 3.** The mean (standard deviation) of measured saturated hydraulic conductivity (K_{sat};

2   mm s^{-1}) and fitted absolute value of saturated matric potential (Ψ_{sat}; mm), fitted pore size

3   distribution parameter (B) and the correlation coefficients (R^2) between calculated matric

4   potential using fitted equations and measured.

Layer (cm)	K_{sat}	Matric potential		
		Ψ_{sat}	B	R^2
0-10	0.0285 (0.0274)	49.14	4.03	0.991
10~20	0.0056 (0.0036)	70.66	4.49	0.996
20-30	0.0047 (0.0027)	27.02	5.22	0.994
40-50	0.0078 (0.0043)	143.4	3.59	0.994
70-80	0.0072 (0.0054)	179.6	3.22	0.993
110-120	0.0315 (0.0054)	603.7	1.89	0.969
150-160	0.0053 (0.0028)	49.17	2.97	0.993
190-200	0.0036 (0.0023)	14.47	4.565	0.989

Table 4. Model performance of substituting default sand parameters with measured porosity (I), thermal conductivity (II), hydraulic conductivity (III) and matric potential (IV) .

	Best	I+II	I +III	I+ IV	II+ III	II+ IV	III+ IV	I+ II+ III	I+ II+ IV	I+ III +IV	II +III +IV	All
100 cm ST	II											
ALD	I		1									
PLB	II	1	2									
10 cm SM	I	7	2	4				1	5	6		3
40 cm SM	I											
80 cm SM	I	7	1	4				2	6	5		3
160 cm SM	I	1										

Note: Best column showed the model simulations (individual parameter substitution) with the smallest root mean squared error (RMSE) for 100 cm soil temperature (ST, ^{o}C), active layer depth (ALD, m), permafrost low boundary (PLB, m), 10, 40, 80 and 160 cm soil liquid water content (SM, -); √ indicated the combination of parameters (+) had smaller RMSE than the best model run using individual parameter substitution.

1 **Table 5** Same as Table 4, but for silty clay.

	Best	I+II	I+III	I+IV	II+III	II+IV	III+IV	I+II+III	I+II+IV	I+III+IV	II+III+IV	All
100 cm ST	I	2		1					3			
ALD	I	4	5	7				1	2	6		3
PLB	II											
10 cm SM	I	7	5	6				4	3	1		2
40 cm SM	I	7	6	4				5	3	2		1
80 cm SM	I											
160 cm SM	I	1	3	4				2	5			

1   **Figure 1. a)** The location of Beiluhe permafrost station on the Qinghai-Tibetan Plateau

2   (Permafrost type is from Li and Cheng, 1996); **b)** the aerial view of the meteorological station

3   and the excavated soil pit; and **c)** the detailed view of the excavated soil pit.
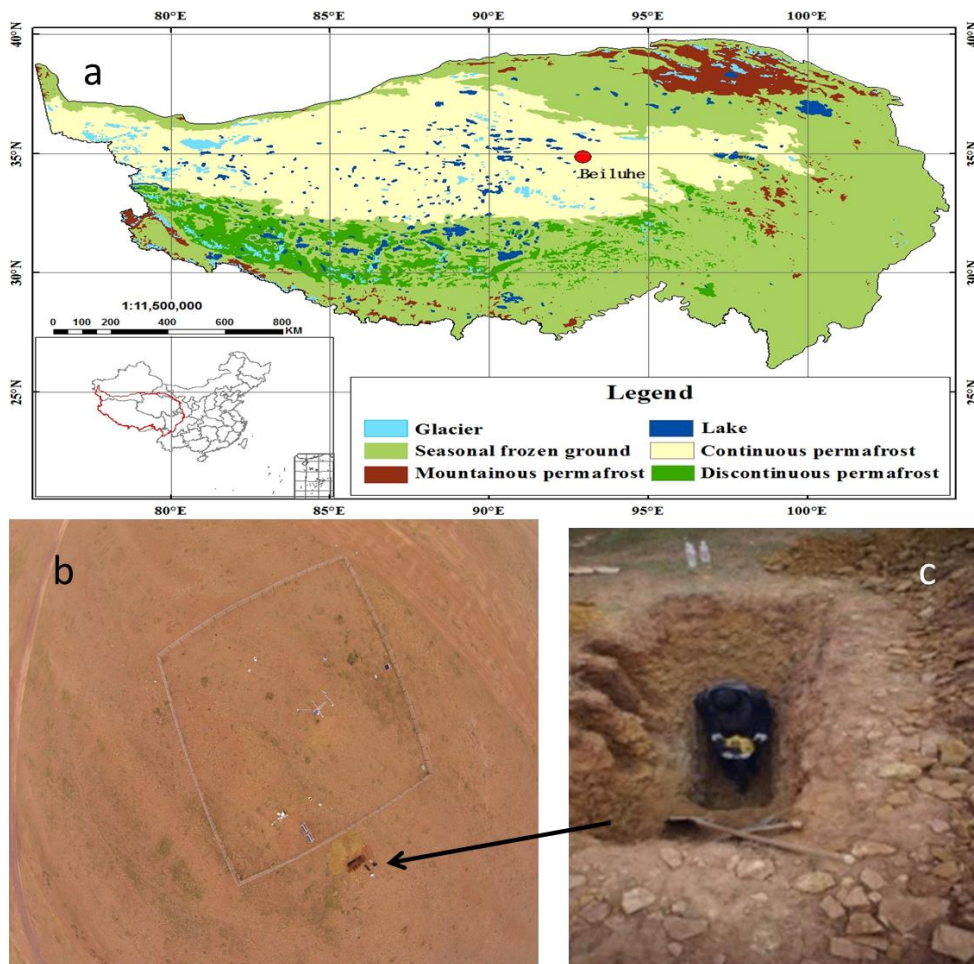
1 **Figure 2.** The relationship between soil wetness (solid and dotted lines represent frozen and

2 unfrozen cases) and soil thermal conductivity (W/m°C) from **a)** measured values (Measured;

3 dots and empty diamonds represent measured frozen and unfrozen soil thermal conductivities,

4 respectively), **b)** using the Côté and Konard (2005) scheme (CK); and **c)** using the Farouki

5 (1986) scheme (Farouki). Thick and thin lines represent relationships for sand and silty clay,

6 respectively.
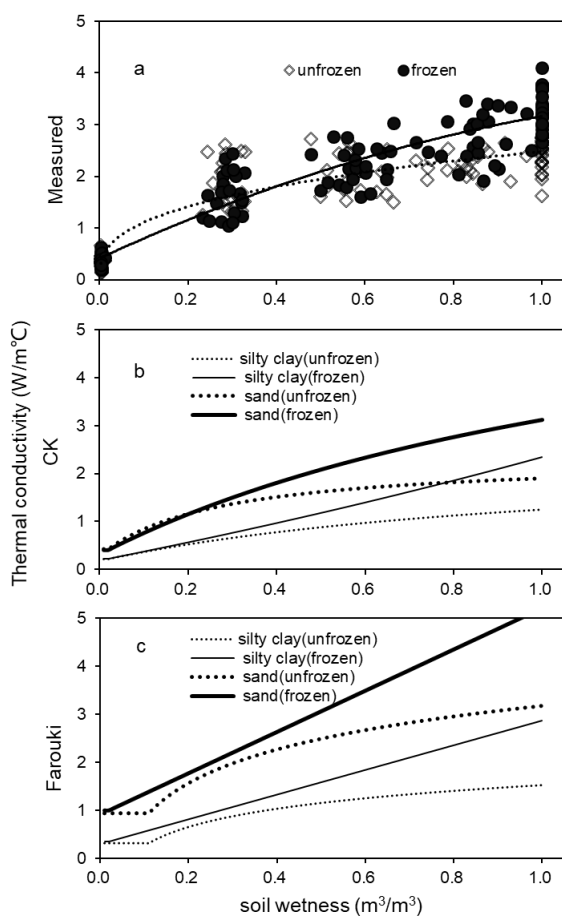
1   **Figure 3**. **a)** the relationship between saturated hydraulic conductivity (mm s^{-1}) and gravel

2   content fraction (Solid dots represent measured value; empty circle and empty triangle

3   represent the corresponding values of sand and silty clay used in Community Land Model,

4   respectively) ; **b)** the relationship between soil wetness (lines) and absolute value of matric

5   potential (mm) at three representative depths. Solid and dashed lines represent default values

6   of sand and silty clay, respectively (Oleson et al., 2014).
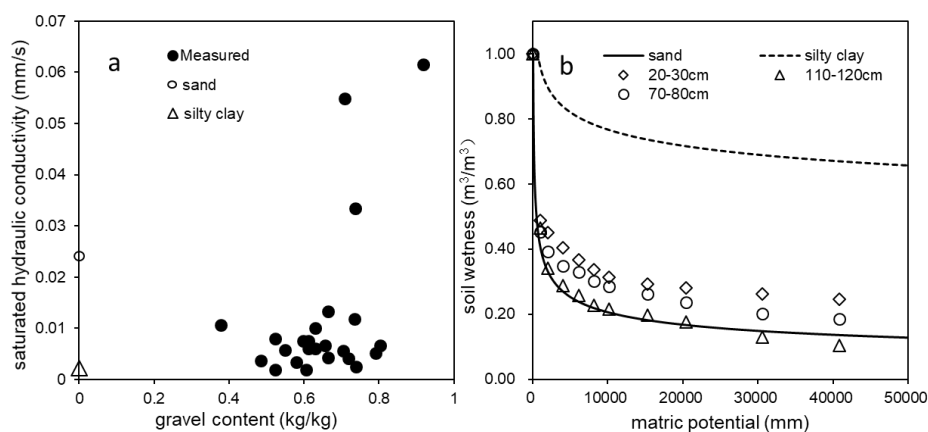
1 **Figure 4.** Comparisons of soil temperatures simulated using default parameters of sand, silty

2 clay, and measured parameters (lines) with measured soil temperatures (dots) at 20, 100, 200

3 and 400 cm depths. Error bars showed the standard deviation calculated based on 9

4 simulations with 3 different slopes and 3 different soil thicknesses.
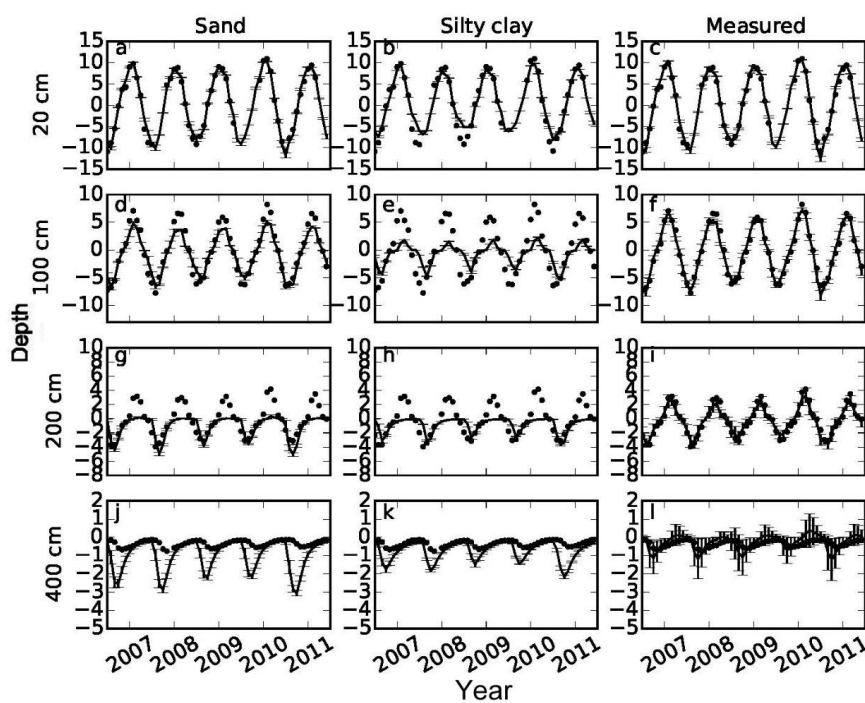
Figure 5. Comparisons of soil volumetric liquid water content simulated using default parameters sand, default silty clay, and measured parameters (lines) with measured soil moistures (dots) at 10, 40, 80 and 160 cm depths. Error bars showed the standard deviation calculated based on 9 simulations with 3 different slopes and 3 different soil thicknesses.
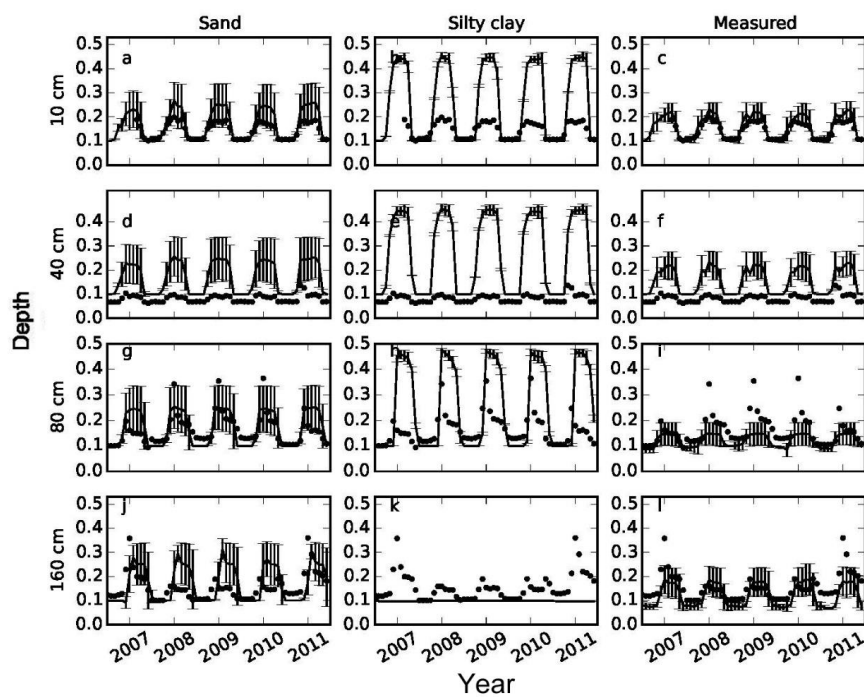
1 **Figure 6. a)** Contours of measured soil temperature (°C) from borehole measurements down
2 to 5 m and simulated active layer depth over the period of 2003-2011; and **b)** same as a) but
3 down to 50 m and for simulated permafrost low boundary. Black, blue and magenta represent
4 simulations with silty clay, sand and measured parameters, respectively. Error bars show the
5 standard deviation calculated based on 9 simulations with 3 different slopes and 3 different
6 soil thicknesses.
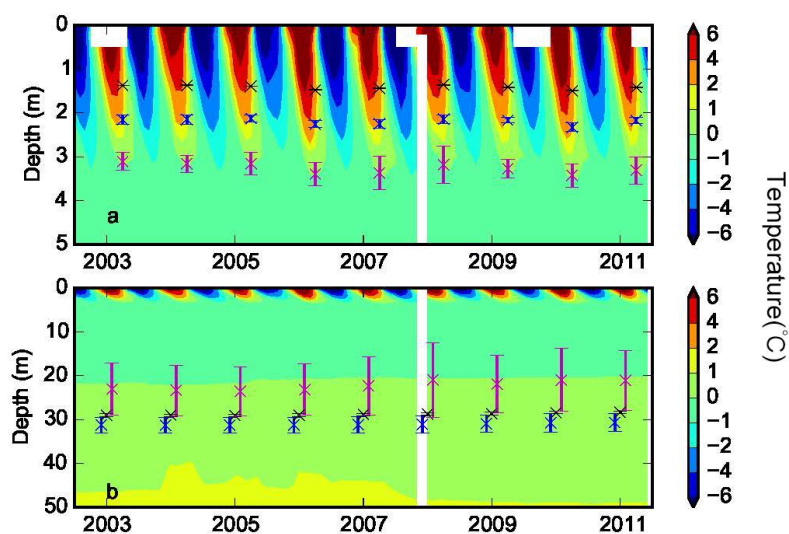
1 **Figure 7.** Root mean squared errors between measurements and model simulations (with

2 different combinations of measured porosity (I), thermal conductivity (II), hydraulic

3 conductivity (III) and matric potential (IV) of default sand parameters) for a) 20 and b) 100

4 cm soil temperatures (^{o}C), c) active layer depth (ALD, m) and d) permafrost low boundary

5 (PLB, m). O and All represent model runs without substitution of default parameters and with

6 all 4 parameters substituted, respectively. Mean and standard deviation of model simulations

7 with 3 different soil thicknesses at each slope are shown.
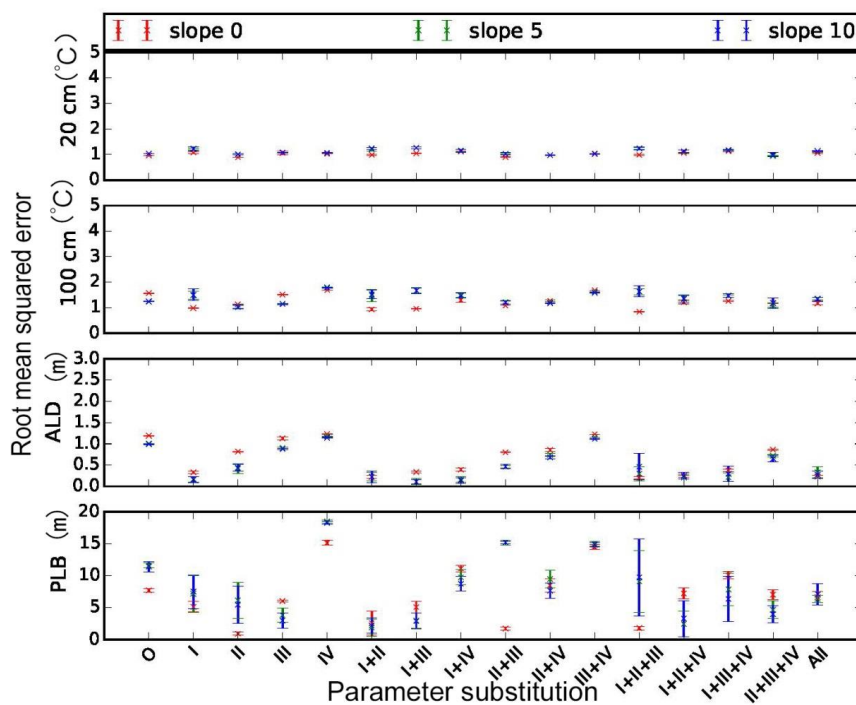
1 **Figure 8.** Same as Figure 7 but for default silty clay parameters.
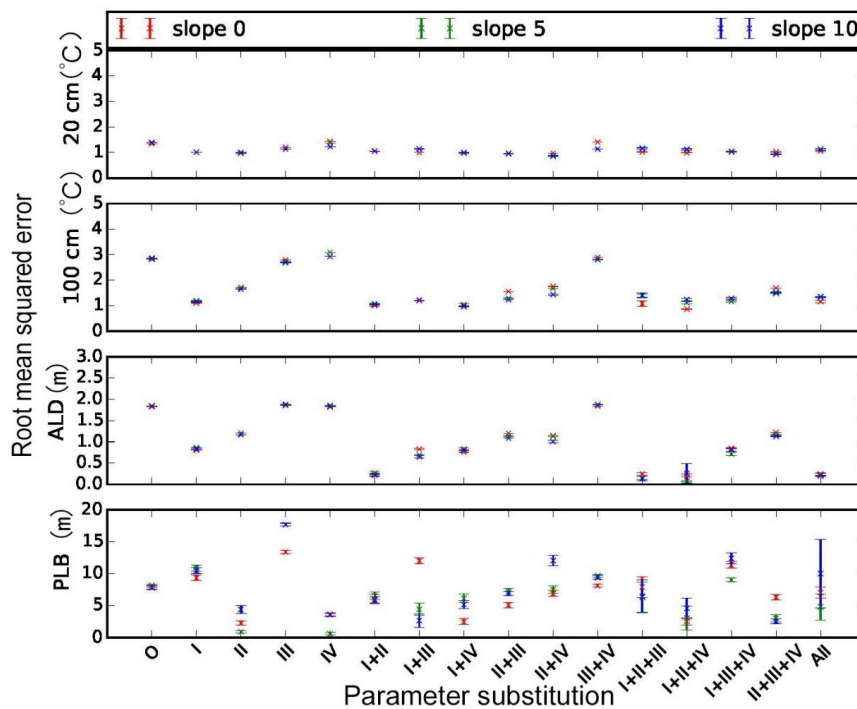
1 **Figure 9.** Same as Figure 7 but for **a)** 10 cm, **b)** 40 cm, **c)** 80 cm and **d)** 160 cm soil liquid

2 water content.
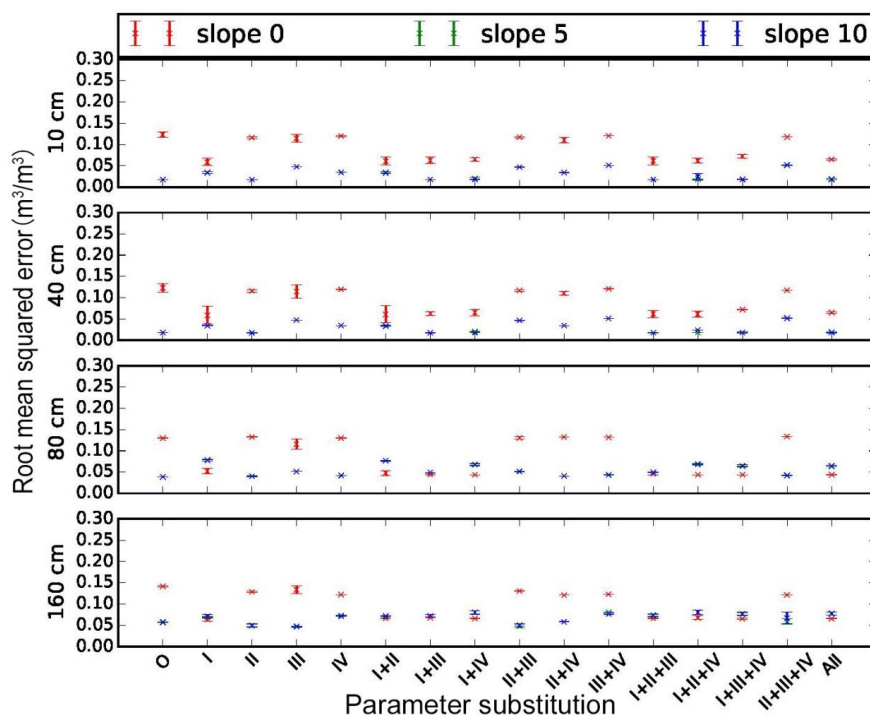
1   **Figure 10.** Same as Figure 9 but for default silty clay parameters.